Sensors and Actuators A 312 (2020) 112155

Contents lists available at ScienceDirect

Sensors and Actuators A: Physical

journal homepage: www.elsevier.com/locate/sna

Adhesion layer-free attachment of gold on silicon wafer and its application in localized surface plasmon resonance-based biosensing

Jay K. Bhattarai, Dharmendra Neupane, Bishal Nepal, Mansour D. Alharthi [1], Alexei V. Demchenko, Keith J. Stine *

Department of Chemistry and Biochemistry, University of Missouri–St. Louis, Saint Louis, MO 63121, USA

ARTICLE INFO

Article history:
Received 18 April 2020
Received in revised form 8 June 2020
Accepted 9 June 2020
Available online 10 June 2020

Keywords:
Plasmonic-active nanostructured thin film
Adhesion layer
Localized surface plasmon resonance
Biosensor
Gold
Silicon

ABSTRACT

The use of a metallic adhesion layer between plasmonic-active nanostructures and a solid support is known to dampen the plasmonic response. To overcome this problem, organic adhesion layers have been introduced, which in turn can undermine the stability of the film. Moreover, both types of layers limit the regeneration of the nanostructures for multiple uses. Here we report a quick and simple approach to prepare intermediate adhesion layer-free binding of nanostructured films of gold on silicon wafers. The approach involves scratching and etching of the silicon wafer before sputter coating with a thin layer of Au. The plasmonic-active nanostructures were then prepared on this thin Au film using electrochemical deposition. As-prepared plasmonic-active nanostructured thin films of gold (PANTF-Au) are easy to handle, physically robust, and can be regenerated. The bulk refractive index sensitivity of PANTF-Au is 150 nm/RIU with the figure of merit 1.4, and with a plasmonic field-decay length of 27 nm. We further used these thin films to study interactions between lectin and glycoprotein inside a flow cell as well as on a microplate made of PANTF-Au. The PANTF-Au can be easily integrated with electrochemical devices and microfluidics, which can help to pave the way toward the development of ideal optical-electrochemical point-of-care biosensors.

1. Introduction

Localized surface plasmon resonance (LSPR) can be supported by nanostructures of different materials such as Au [1], Ag [2], Cu [3], C (e.g., graphene) [4], Al [5], TiN [6], and alloys or composites of these materials [7]. However, the most interesting and investigated nanostructures for LSPR-based biosensing are based on Au. Nanostructures of Au have many important properties required for designing an ideal LSPR-based biosensor. The LSPR peak of these nanostructures can be tuned from visible to near infrared wavelengths by simply controlling their shape and size [8]. They can be modified by self-assembled monolayers (SAMs) of thiolated organic molecules, which can be used for immobilizing bioreceptors or directly capturing analytes [9,10]. They are also biocompatible, chemically inert, and can be regenerated. Recently, the focus has been shifted from discrete Au nanostructures to plasmonic-active nanostructured thin films of Au (PANTF-Au) mainly because of three key reasons: (1) these can simultaneously generate both surface plasmon polaritons (SPP) and LSPR [11,12], (2) these can yield largely enhanced signals in surface-enhanced Raman spectroscopy (SERS) [13,14], and (3) they are conductive. Because of these reasons, there is a strong possibility of integrating PANTF-Au into different optical and electrochemical label-free biosensing techniques.

The PANTF-Au on a suitable solid support can be prepared by applying different strategies before, during or after the deposition step [7]. The shape and size of nanostructures on the film can be controlled by predesigning the solid support using template-based techniques such as electron beam lithography (EBM), nanosphere lithography (NSL), nanoimprint lithography, and porous membrane-based lithography. A thin layer of Au can then be sputter or vapor deposited on the as-prepared solid support to create PANTF-Au. Controlling the deposition parameters, such as deposition angle, time and temperature, can introduce diversity to the nanostructures of the film. The nanostructures can also be constructed by post deposition treatment of the Au film such as thermal annealing, electrochemical deposition, and ion-beam lithography. However, the deposited Au films do not bind strongly to the silicon or glass support. For the PANTF-Au to be used as a

* Corresponding author.
E-mail address: kstine@umsl.edu (K.J. Stine).
[1] Present address: King Saud University, Riyadh, Saudi Arabia 11451.

https://doi.org/10.1016/j.sna.2020.112155
0924-4247/

transducer of a biosensor, it should not only be sensitive but also be physically stable under the operating conditions. However, the trade-off between physical stability and sensitivity of PANTF-Au is an obvious hindrance for the development of ideal LSPR-based biosensors.

The common strategies for preparing PANTF-Au on silicon or glass substrates involve using either a metallic (e.g., Cr and Ti) or an organic (e.g., silanes and polymers) adhesion layer between PANTF-Au and substrate [15,16]. However, metals used as an adhesion layer have been known to dampen the LSPR signal and interfere with SERS enhancement [17]. Additionally, they lower the coverage of biological molecules due to interference in self-assembled monolayer formation. When used along with electrochemical techniques they can form a galvanic cell, which may interfere with the electrochemical response [18]. On the other hand, silanes having terminal thiol or amine group are also commonly used intermediate organic molecules for attaching gold nanostructures onto silicon through the formation of an oxides or hydroxides layer on the silicon surface [15,19]. Although these molecular linkers act as a non-damping alternative to metal adhesion [20], they are not free from limitations. Alternatively, we used epoxy as an adhesion layer for attaching Au film on Si-wafer in our earlier work [1]. The stability of these organic adhesion layers, however, is weaker compared to metallic adhesion layer and are also less compatible with solvents and electrochemical potentials required for the regeneration of these surfaces.

PANTF-Au on a silicon substrate has been extensively used as a transducer for bioassay and biosensing applications, for example, patterning the surface with biomolecules, determining the binding constants of the interactions of different biomolecules, and label-free detection of bacteria, virus, and disease biomarkers (e.g., proteins and DNA) [21–23]. In addition to biosensing, stable Au films on silicon surfaces have widespread application in different technologies. For example, it is widely used in soft lithography for micro- and nano-scale patterning [24], and for attaching an integrated circuit on the circuit board [25]. Despite the importance of intermediate adhesion layer free attachment of Au and silicon, a suitable strategy for preparation at low temperature is lacking. Si-Au binding can be attained by heating 18.6% Si and 81.4% Au at the eutectic temperature of 363 °C [26]. However, these conditions are not desirable for making PANTF-Au as the thin film converts to island-like structures due to dewetting.

Here, we report a simple approach to creating strong Si-Au binding by roughening the Si wafer surface before Au deposition. The roughening process creates surface defects on the wafer surface enhancing nucleation sites, which improves the adhesion of Au thin films. We used as-prepared thin film to electrochemically prepare PANTF-Au and demonstrated its sensitivity to study lectin-glycoprotein interactions inside a home-built flow cell and on a microwell plate made of PANTF-Au using LSPR-based biosensing. This work could be a potential solution for certain obstacles, such as lack of stability and reusability of a transducer as well as multiplexing capacity, and for improvement and commercialization of miniaturized point-of-care (POC) devices, as depicted in Scheme 1.

2. Experimental section

2.1. Materials

Silicon wafers (3'' N<100>, 1–10 ohm-cm, 356–406 μm thick) prime grade were purchased from Nova Electronic Materials, LLC (Flower Mound, TX). Sodium hydroxide, potassium dicyanoaurate(I), glycerol, 11-mercaptoundecanoic acid (MUA) and N-hydroxysuccinimide (NHS), poly(allylamine hydrochloride) (PAH, 65 kDa), poly(sodium-4-styrenesulfonate) (PSS, 70 kDa) were purchased from Sigma-Aldrich, Inc. (Milwaukee, WI). Bovine serum albumin (BSA), Ovalbumin (OVA), Concanavalin A (Con A), α-1 acid glycoprotein (AGP), tris buffer, and N-(3-dimethylaminopropyl)-N′-ethylcarbodiimide hydrochloride (EDC) were purchased from Sigma-Aldrich, Inc. (Saint Louis, MO). *Sambucus nigra* agglutinin (SNA) was purchased from Vector Laboratories (Burlingame, CA). Milli-Q water (18.2 MΩ cm) was used for making all aqueous solutions.

2.2. Preparation of thin Au film

The surface of a silicon wafer was scratched with fine grade (1000–3000 grit) silicon carbide abrasive sheet (3M™) in a circular motion until the shiny luster of the Si wafer disappears. Next, the wafer was etched by submerging in 10 M NaOH for 20 min at room temperature. Then the surface was thoroughly cleaned with Milli-Q water, rinsed with chloroform first and then with methanol, dried at 110 °C for 10 min and quickly transferred to the sputter coater (Hummer VI, Anatech Ltd). The wafer was sputter coated with Au for 20 min adjusting the current to 10 mA to obtain a thickness of about 200 nm, which produces a film of good surface quality with minimum patches of holes between Au islands. The as-prepared thin film was left at least 17 h at room temperature for improving stability before electrodeposition.

2.3. Preparation of PANTF-Au

A 273A potentiostat (EG&G Princeton Applied Research) was used for electrodeposition of nanostructured Au onto thin Au film to create PANTF-Au. For all the electrochemical experiments, a standard three-electrode electrochemical setup was used with a sputtered thin Au film working electrode, Ag/AgCl (satd. KCl) reference electrode, and platinum wire (99.997% purity, 0.5 mm diameter) counter-electrode. Nanostructures were created on the sputtered thin Au film by applying a potential of −1.2 V for 60 s followed by −1.6 V for 30 s using 50 mM potassium dicyanoaurate(I) electrolyte in 0.25 M sodium carbonate at room temperature.

2.4. Characterization

2.4.1. Scanning electron microscopy (SEM) imaging

The morphology of the samples was characterized using a field emission scanning electron microscope (6320 F, JEOL USA, Inc.). Images were acquired at a working distance of 8 mm at an accelerating voltage of 8 kV and processed using ImageJ. Elemental analysis of the samples was carried out using the energy dispersive X-ray (EDX) spectrometer interfaced to the SEM.

2.4.2. Atomic force microscopy (AFM) imaging

AFM images were collected for characterizing morphology of scratch and scratch-etched Si wafer. NanoScope III microscope (Digital Instruments, Inc., Santa Barbara, CA) and silicon cantilevers TAP300Al-G (Ted Pella, INC, Redding, CA) having force constant 40 N/m and resonance frequency of 300 kHz were used for imaging in tapping mode. The images were processed using Gwyddion software.

2.4.3. XRD and contact angle measurement

The crystallinity of sputtered thin Au film and PANTF-Au were compared using a X-ray diffractometer (XRD, Ultima IV, Rigaku) with Cu Kα radiation (λ =1.5406 Å). The contact angles were determined using a home-made setup and ImageJ software, as reported in our previous work [9].

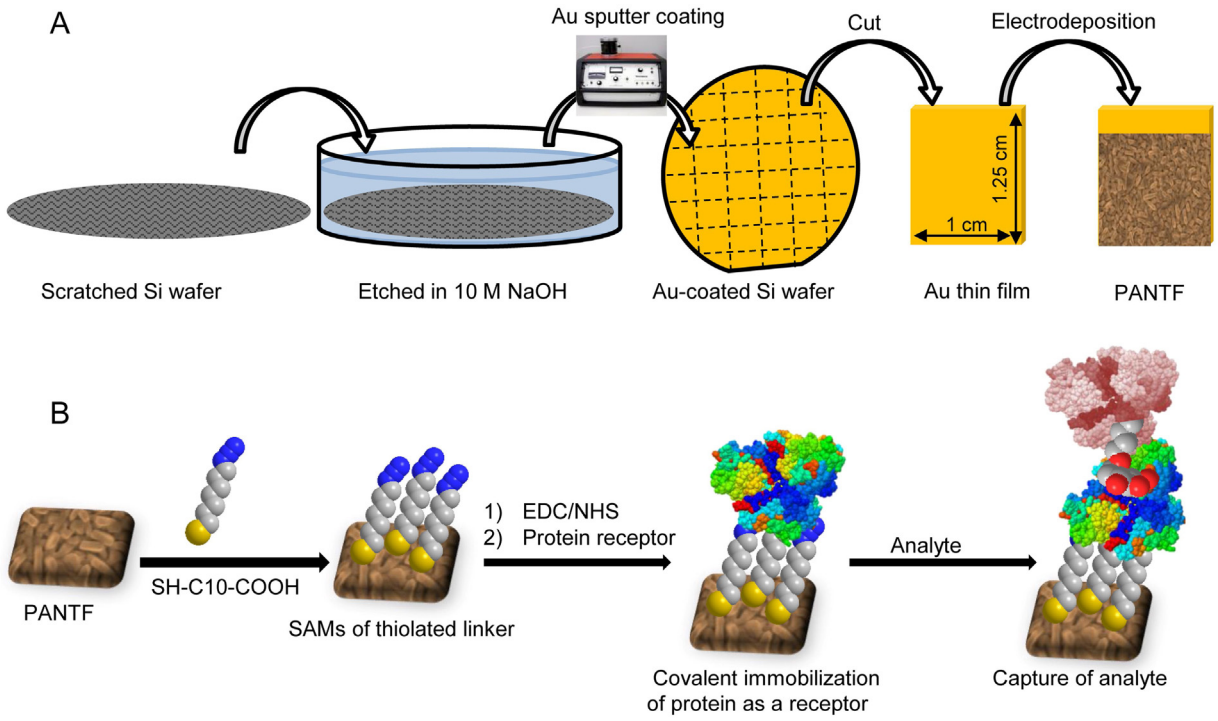

Scheme 1. Schematic diagram of (A) plasmonic-active nanostructured thin film of gold (PANTF-Au) fabrication strategy and (B) transducer functionalization and analyte capture process.

2.4.4. Electrochemical measurements

Electrochemical measurements were performed using a PARSTAT 2273 potentiostat (EG&G Princeton Applied Research). The formation of SAM on PANTF-Au was determined by electrochemical impedance spectroscopy (EIS) in 5 mM $K_3[Fe(CN)_6]/K_4[Fe(CN)_6]$ prepared in PBS buffer over the frequency range of 1–10^5 Hz, bias potential of 0.2 V (vs. Ag/AgCl), and an AC amplitude of 10 mV. The Nyquist plots of EIS were analyzed using ZSimpWin software by fitting to the Randles equivalent circuit, R(Q[RW]). The surface coverage of SAMs on PANTF-Au was determined using cyclic voltammetry (CV) in 0.5 M NaOH by scanning from −0.200 to −1.4 V at a scan rate of 100 mV s^{-1}.

2.4.5. LSPR analysis

All the LSPR spectra were recorded using UV–vis reflection geometry. The setup consists of a light source (DH-2000-BAL, Deuterium-Halogen Light, Ocean Optics), spectrometer (Jaz, Ocean Optics), a reflection probe (Ocean Optics, QR400-7-SR), and a home-built Teflon flow cell (volume 600 μL) with a quartz window or a microwells designed on PANTF-Au (volume 10 μL). The distance between probe and the PANTF-Au surface was kept constant to 4 mm. The reflection spectra obtained were plotted as reciprocal reflectivity versus wavelength using SigmaPlot 12.0 (Systat Software Inc.).

2.4.5.1. Determination of bulk refractive index sensitivity (RIS). The bulk RIS of the PANTF-Au was determined by recording the reflection percentage spectra by passing different concentrations of glycerol solution (0%, 15%, 30%, 45%, 60%, and 75% by weight) over PANTF-Au inside flow cell. The refractive index values of the glycerol solutions are 1.33, 1.35, 1.37, 1.39, 1.41, and 1.43, respectively [1].

2.4.5.2. Determination of electromagnetic-field decay length. The PANTF-Au inside the flow cell was functionalized with SAM of cysteamine by injecting 1 mM cysteamine solution in ethanol for 1 h followed by rinsing with ethanol and water. Polyelectrolyte multilayers of PSS and PAH were formed on top of cysteamine by alternatively injecting 1 mg/mL PSS and PAH solution in 0.1 M NaCl. The injected polymer solution was left undisturbed for 15 min to allow electrostatic interactions followed by rinsing with water and drying using nitrogen before acquiring LSPR spectra.

2.4.5.3. Biosensing. The SAM of MUA was prepared on PANTF-Au by immersing freshly prepared PANTF-Au in 0.20 mM MUA in ethanol for 17 h at room temperature. To study the OVA–Con A interactions inside flow cell, the terminal carboxyl group of the functionalized MUA was activated with a mixture of 0.2 M EDC and 0.05 M NHS in MES buffer pH 6.4 for 15 min. The glycoprotein OVA was then covalently immobilized on the activated surface by injecting 50 μg/mL OVA in HEPES buffered saline pH 7.4 for 1 h. Finally, the lectin Con A in TRIS buffer was captured on immobilized OVA, rinsed with TRIS followed by water. The spectra were recorded after SAM formation, OVA binding, and Con A capture under N_2 environment.

A rapid drop test was performed to detect glycoprotein AGP on microwells designed on PANTF-Au that were functionalized with lectin SNA. Protein immobilization strategies discussed above were also utilized for immobilizing SNA on PANTF-Au except performed outside in a small beaker. The unreacted terminal esters were capped with ethanolamine (1 M pH 8.0) and rinsed with water. The as-prepared biosensor chip was sandwiched between layers of gaskets and Teflon plates with four holes on one side of the gasket and Teflon. These holes were used for directing the incident light to the sample as well as maintaining the distance between probe and sample. Capture of AGP by SNA was achieved by adding different concentration of 10 μL droplet of AGP (PBS pH 7.4) inside microwells and cleaning with PBS buffer after 1 h of incubation. Before taking the LSPR spectra the PANTF-Au were rinsed with water and dried with N_2.

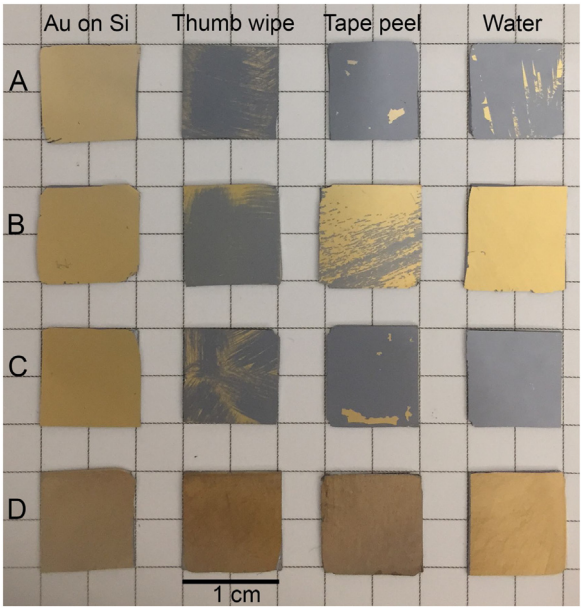

Fig. 1. Photographic image of (Column 1) sputtered Au thin film on Si wafer and (Column 2–4) after wiping with thumb, scotch tape peeling test, and dipping in H_2O for 17 h, respectively. The Si wafer substrates used were (A) as-purchased, (B) scratched with abrasive sheet, (C) etched with 10 M NaOH for 20 min, and (D) both scratched and etched.

3. Results and discussion

3.1. Fabrication and stability of thin film of Au on Si wafer

We sputter deposited thin films of gold on unmodified and modified (scratched, etched, and scratched–etched) Si wafer. The stability of the as-deposited Au thin film on unmodified and modified Si wafer was tested after 17 h of deposition using different simple methods. Fig. 1 shows that the thin film easily peels off the as-purchased Si wafer when rubbing with a thumb, peeling with a tape or submerging in water overnight (row A). However, roughening the Si wafer surface using an abrasive sheet was found to slightly improve the stability of film to tape and water (row B). Unlike scratching, etching the Si wafer surface with 10 M NaOH for 20 min did not improve the stability of the film (row C). Interestingly, scratching followed by etching dramatically improved the stability of sputtered thin Au film on all the three tested conditions (row D). However, it should be noted that when the thumb and tape test were performed on wet film, the film was easily delaminated. Also, etching followed by scratching slightly improved the stability of the film but not as effectively as scratching followed by etching.

3.2. Characterization of scratched and scratched-etched Si wafer

The morphology of scratched and scratched-etched Si wafer was imaged by SEM and AFM imaging for understanding the reason behind stable Au thin film attachment on the scratched-etched surface. The SEM (Fig. 2A–B and Figure S1A) and AFM (Fig. 2C) images of the scratched surface show smoother morphology compared to the scratched-etched surface (Fig. 2D–F and Figure S1B). The low and high magnification SEM images of the scratched-etched surface show patches of the planar (dark) and island-like (bright) structures. The AFM image shows granular structures on island-like features, whereas the line profile indicates deeper grooves on the scratched-etched surface. The 3D AFM image shows increased roughness for the scratched-etched Si wafer surface compared to scratched only (Figure S2). The formation of island-like structure, granularity, and deeper crevices on scratched-etched surfaces improved the stability of the Au film attachment on its surface by enhancing nucleation sites for Au atoms for Au film formation.

3.3. Characterization of sputtered Au thin film

Although the features on the Si surface are important for the stability of the Au thin film, they are not the only parameters involved in the stabilizing process. We found that the stability of the sputtered Au thin film increases with time at room temperature. Fig. 3 shows SEM images of Au thin film on scratched-etched Si wafer instantly after deposition and after leaving them for 17 h at room temperature. It can be seen that the sputter-coated Au film initially contains granular structures separated from each other, which diffuse and merge with time to form a monolithic structure. This type of phenomenon on deposited gold has been observed before during annealing at high temperature [27]. However, on the surface of the scratched-etched Si wafer annealing of Au grains happens at room temperature, improving the stability of the film. Therefore, both the roughness of the Si wafer surface as well as the nucleation process of gold are important factors for the stability of the Au thin film.

3.4. Real-time determination of deposition conditions for PANTF-Au formation

Fig. 4A is a schematic diagram of the setup of optical and electrochemical techniques for the real-time determination of optimal electrochemical deposition conditions. This setup helps to monitor the LSPR peak as the nanostructures start to form on the surface of the thin film. As shown in Fig. 4B, the LSPR peak can be monitored in real time during the electrodeposition. To check the effectiveness of this setup, we used the two-step chronoamperometric technique with the conditions optimized from our previous work, which is providing the potential of −1.2 V for 60 s followed by −1.6 V for 30 s. As we provided the potential, the spectra were recorded every 10 s for 120 s, the chronoamperometric curve is included with supporting information (Figure S3). A distinct LSPR peak appears at 565 nm at the previously optimized condition supporting our previous result. Further increasing the deposition time from optimized conditions decreases the peak intensity and hence the figure of merit. It should be noted that the LSPR spectra are obtained in the presence of electrolytes, and the Au thin film before the deposition was used as a reference surface.

Although this experiment was performed for making PANTF-Au, the procedure can be easily applied to prepare sensitive PANTFs of other materials (e.g. Ag, Cu, Al, etc.). It can also be used to explore different other types of PANTF-Au using additives in the deposition solution. Furthermore, this approach can be applied to tune the LSPR peaks position of nanostructures across the visible and near infra-red region of the electromagnetic spectrum.

3.5. Characterization of PANTF-Au

Fig. 6A is an SEM image of PANTF-Au prepared using optimal electrochemical deposition conditions, −1.2 V for 60 s followed by −1.6 V for 30 s in 50 mM $KAu(CN)_2$ and the inset is a magnified image. It shows randomly oriented brick-like nanostructures with a length of nearly 200 nm and a width of 100 nm. It is noteworthy that the PANTF-Au is free from cracks and defects over a large area. The XRD data shows an increase in the crystallinity of the PANTF-Au than that of the sputtered Au thin film as shown in Fig. 5B. The small contact angle of water on PANTF-Au ($46^\circ \pm 4$) compared to that of sputtered Au thin film ($93^\circ \pm 2$) proves improved wettability of the PANTF-Au surface, Fig. 5C.

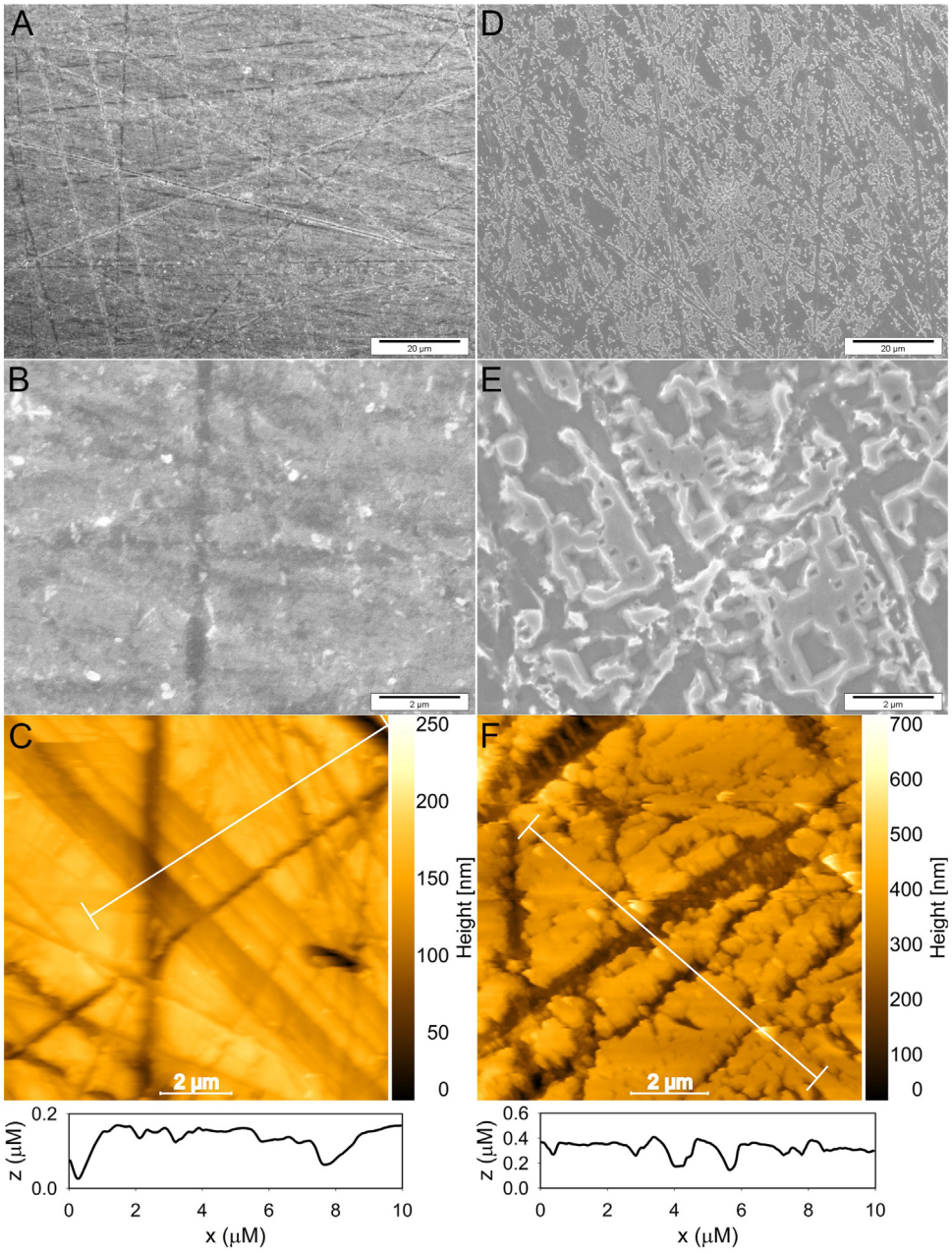

Fig. 2. (A–B) SEM images at low and high magnification and (C) AFM topographical image of scratched Si wafer. (D–E) SEM images at low and high magnification and (F) AFM topographical image of scratched-etched Si wafer. Below the AFM images are their corresponding line profiles.

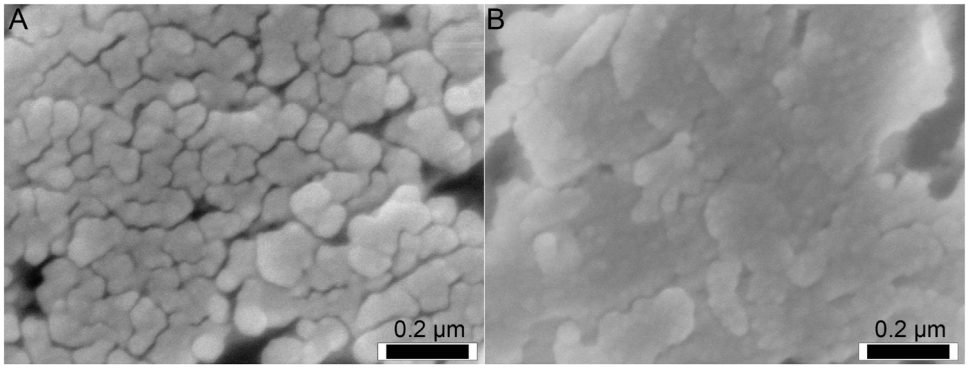

Fig. 3. SEM images of Au thin films sputter deposited on scratched-etched Si wafer surface (A) instantly after deposition and (B) after 17 h at room temperature.

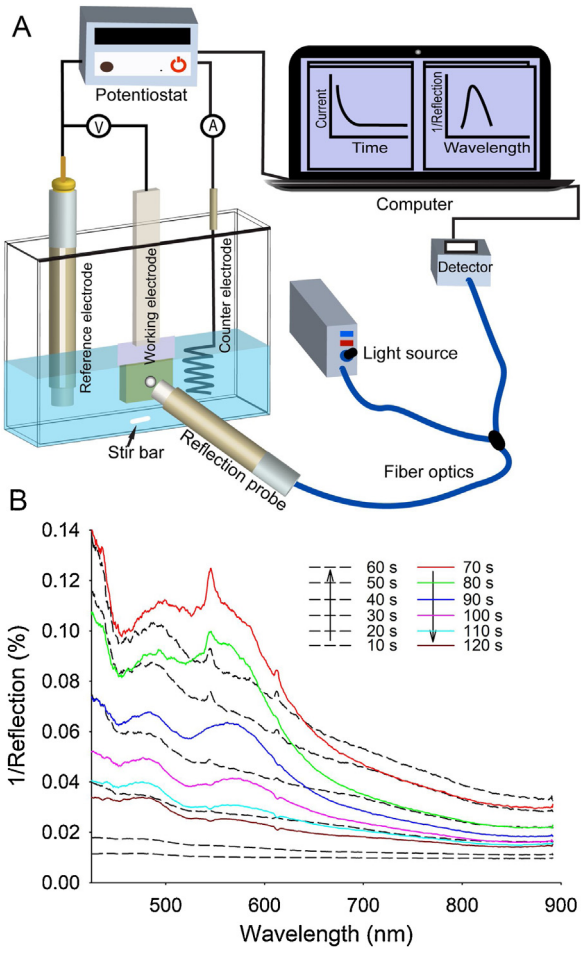

Fig. 4. (A) Schematic of setup for the real-time monitoring of LSPR peak with the formation of Au nanostructrues on thin film. (B) Monitoring the LSPR peak with deposition time in 10 s increament when potential of −1.2 V (vs. Ag/AgCl) for 60 s followed by −1.6 V (vs. Ag/AgCl) for 30 s were applied.

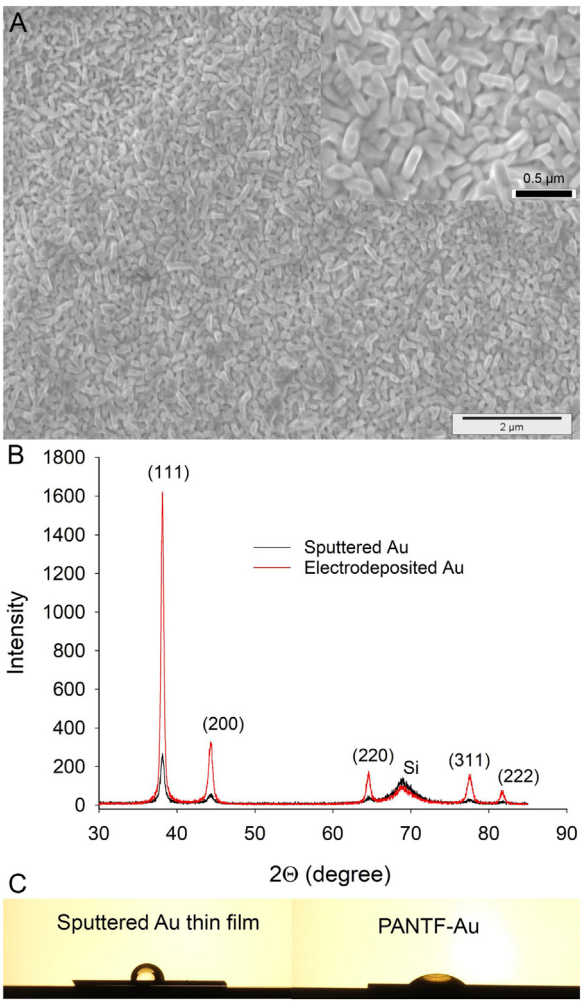

Fig. 5. (A) SEM image of PANTF-Au prepared using two step chronoamperometry technique (−1.2 V for 60 s followed by −1.6 V for 30 s in 50 mM $KAu(CN)_2$). (B) and (C) are XRD and contact angle measurement of the sputtered Au thin film and electrodeposited PANTF-Au, respectively.

3.6. Determination of bulk RIS and field decay length

The change in peak wavelength and intensity of PANTF-Au is a linear function of the refractive index of the surrounding solution. We injected aqueous glycerol of varying concentration (0–75%) in a series through PANTF-Au inside the flow cell. The corresponding spectra as a result of the change in refractive index were recorded as shown in Fig. 6A. Fig. 6B shows a linear increase in wavelength and intensity over a wide range of refractive index (1.33–1.43), and the slope of plots gives values of the bulk RIS. The bulk RIS is an important parameter for determining and comparing the sensitivity of plasmonic-active nanostructures for sensing, and for our PANTF-Au it is 150 ± 2 nm/RIU and 0.050 ± 0.005 response/RIU in term of wavelength and reciprocal reflectivity, respectively. The RIS values of PANTF-Au are significantly higher compared to previously reported values of nanostructures of gold that have similar peak wavelengths in air or nitrogen (~520–530 nm) [1,28]. This improvement in the bulk RIS compared to that of our previously reported nanostructured thin film (100 nm ± 2 nm/RIU) should be due to roughness of the sputter-thin film due to scratching and etching. The figure of merit (FOM), which is the bulk RIS per full-width at half maxima (FWHM), for PANTF-Au is 1.4.

Although the bulk RIS value provides the sensitivity of the PANTF-Au, determining the electromagnetic field decay length (l_d) is essential to understand the response of PANTF-Au with the change in local refractive index and using it as a transducer for biosensing [29]. We used the following simplified equation to determine l_d [30,31].

$$\Delta\lambda max = m\Delta\eta[1-\exp(^{-2d}/_{l_d})] \quad (1)$$

where $\Delta\lambda max$ is a shift in wavelength, m is the bulk RIS, $\Delta\eta$ is a change in refractive index, and d is the thickness of adsorbate. To control the thickness in the vicinity of the PANTF-Au surface, positively and negatively charged polyelectrolyte polymers were electrostatically assembled in layer-by-layer (LBL) fashion. We started by preparing SAMs of cysteamine on the PANTF-Au surface to create a positive charge followed by the LBL assembly of PSS and PAH. Each polymer bilayer adds a thickness of nearly 2 nm. Fig. 6C shows the redshift in LSPR spectra with the addition of polymer bilayers, and Fig. 6D is a shift in peak wavelength as a function of polymer thickness. Using Eq. (1), the value of l_d was estimated to be 27 nm, which is in agreement with the literature values of 10–30 nm for different types of plasmonic nanostructures [32].

When increasing aqueous glycerol solutions of increasing concentration were passed over the PANTF-Au surface without drying the surface, we have consistently observed an increase in both peak wavelength and intensity. However, when the polyelectrolyte bilayers were immobilized on PANTF-Au and the spectra were recorded after drying the surface with nitrogen, only the wave-

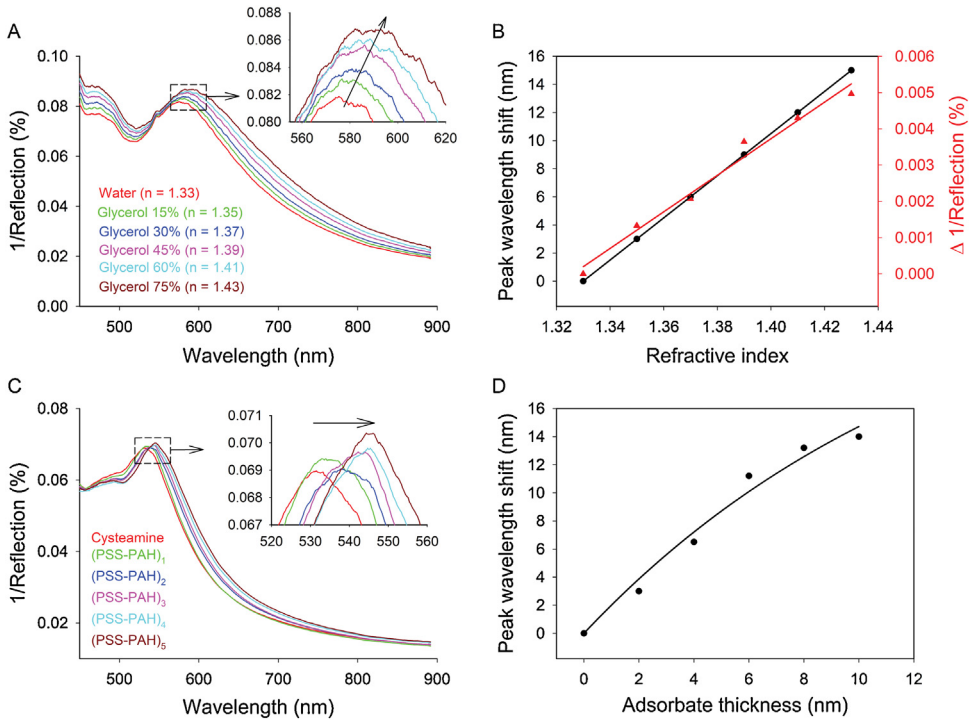

Fig. 6. (A) LSPR spectra of PANTF-Au when immersed in liquids of different refractive indices prepared by varying the concentration of glycerol (0–75% w/w). (B) The shift in peak wavelength or reciprocal reflectivity as a function of refractive indices of the liquids. The data were fitted using linear regression and the slope of straight lines gives bulk RIS of PANTF-Au, which is 150 ± 2 nm/RIU and 0.0504 response/RIU for wavelength and reciprocal reflectivity, respectively. (C) LSPR spectra of PANTF-Au after the formation of bilayers of polyelectrolyte polymers PSS and PAH. (D) The shift in peak wavelength as a function of thickness of polymers. The thickness of each bilayer is about 2 nm. The data were fitted using nonlinear regression ($\Delta\lambda max = m\Delta\eta[1 - \exp(-2d/l_d)]$), which gives a field decay length of 27 nm. The insets on (A) and (C) are magnified regions near peaks of the corresponding figure.

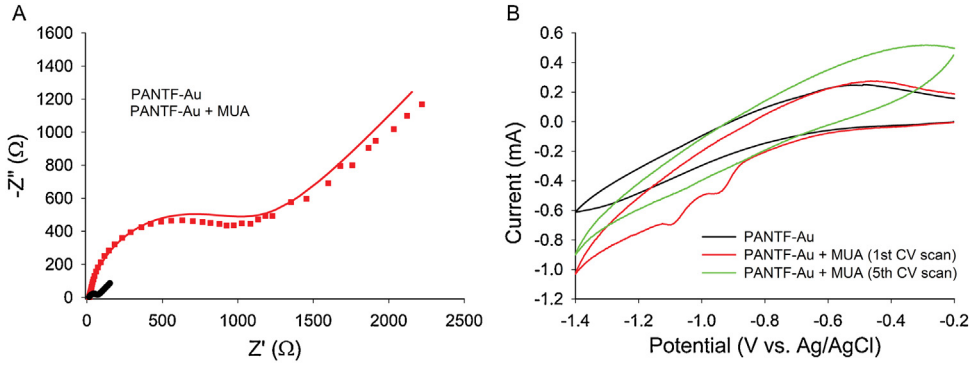

Fig. 7. (A) Nyquist plots of PANTF-Au before (black) and after (red) the formation of SAM of MUA. Symbols represent the experimental data and lines represent fit of the data by Randles equivalent circuit, R(Q[RW]). (B) Cyclic voltammogram of blank PANTF-Au (black) and after reductive desorption of SAM, one cycle (red) and five cycle (green). The CV were obtained at 0.1 V s^{-1} in 0.5 M NaOH. (For interpretation of the references to colour in this figure legend, the reader is referred to the web version of this article.)

length increased consistently but not the reciprocal reflectivity. The frequent inconsistency in the shift in reciprocal reflectivity has also been observed previously and should be used cautiously to study biomolecular interactions [33].

3.7. SAM formation and surface coverage

The important step toward designing a biosensor is to effectively functionalize the transducer with a suitable bioreceptor. We prepared a self-assembled monolayer of MUA on PANTF-Au to covalently capture proteins (e.g., glycoprotein and lectin) to be used as a bioreceptor. Because of the conductive nature of PANTF-Au, we can employ electrochemical techniques to characterize surface modification steps. Fig. 7A shows representative Nyquist plots of blank PANTF-Au and SAM-functionalized PANTF-Au. The charge-transfer resistance (R_{ct}), corresponding to a diameter of a semicircle region of a Nyquist plot, was compared before and after SAM formation. The bare PANTF-Au has R_{ct} of 55 ± 6 Ω, which increases to 1013 ± 46 Ω after dipping the PANTF-Au in 0.2 mM MUA solution suggesting the formation of SAM of MUA. A relatively low concentration of MUA (0.2 mM) was used unlike the commonly used concentration (1 mM) for making SAM to avoid multilayer formation due to hydrogen bonding.

Once the SAM formation on PANTF-Au was confirmed using EIS, the surface coverage of the SAM on the PANTF-Au was estimated using the reductive desorption technique, Fig. 7B. Using the specific surface area of the PANTF-Au (1.46 cm^2), determined using the oxide stripping method [1], and charge under the reduction peak of cyclic voltammogram, the surface coverage of MUA was determined to be 4.72 ± 0.03 molecules/nm^2. This confirms

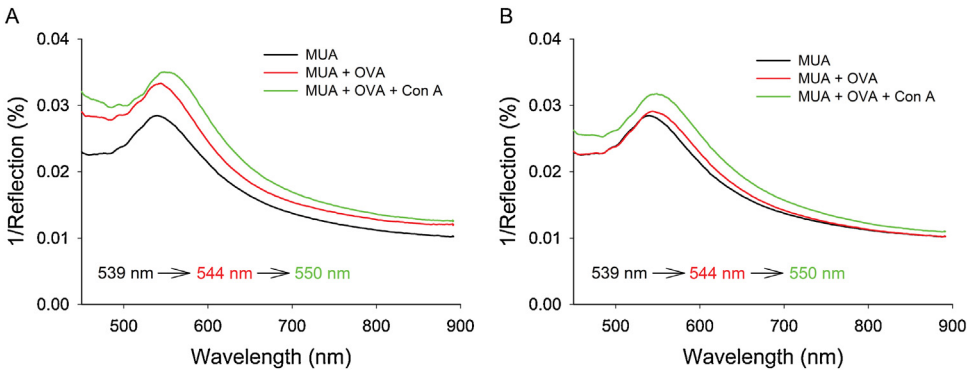

Fig. 8. (A) LSPR spectra of freshly prepared PANTF-Au after modification with different molecules for studying interactions of OVA and Con A: 11-mercaptoundecanoic acid (black), OVA (red), and Con A (green). (B) LSPR spectra of the same PANTF-Au after regeneration and modification. Spectra were collected in a N_2 environment. (For interpretation of the references to colour in this figure legend, the reader is referred to the web version of this article.)

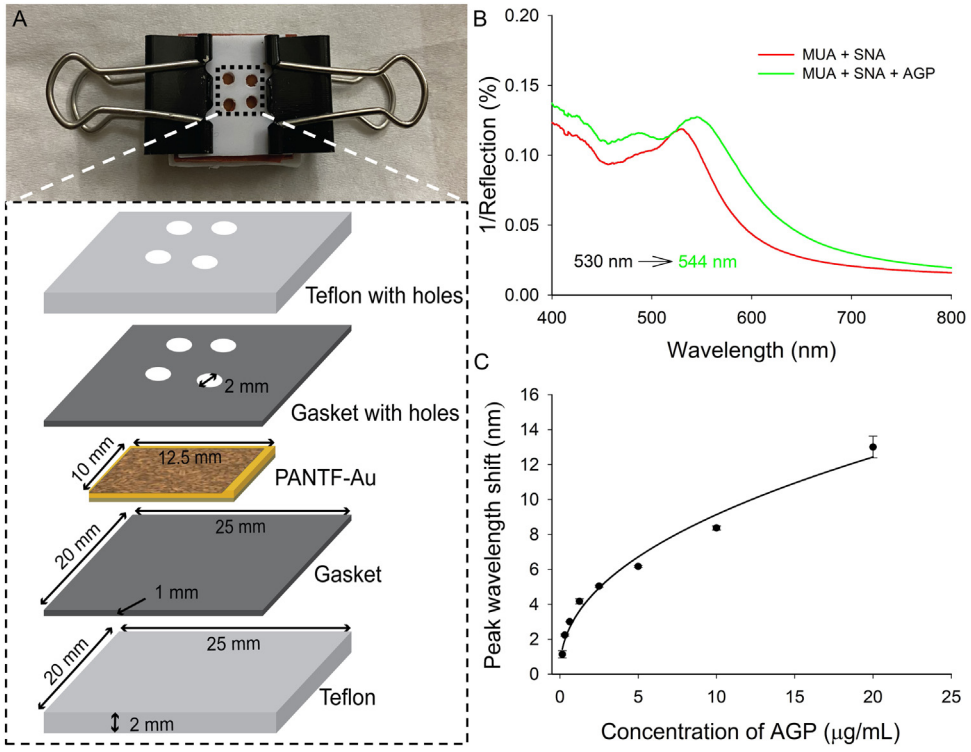

Fig. 9. (A) Photographic image and schematic diagram of setup of droplet-based LSPR biosensor. The PANTF-Au was divided into four microwells making holes on gasket and Teflon plate. (B) LSPR spectra illustrating the response of the PANTF-Au before (red) and after (green) the capture of 20 μg/mL AGP on SNA-functionalized PANTF-Au. (C) LSPR peak wavelength shift as a function of change in concentration of AGP. The solid line is a fitting to Eq. (1). Spectra were collected after drying under N_2. (For interpretation of the references to colour in this figure legend, the reader is referred to the web version of this article.)

highly dense SAM formation on PANTF-Au with the packing density comparable to perfectly formed alkanethiol monolayers on a flat gold surface (~4.5 molecules/nm^2) [34]. The slightly higher coverage of SAM on PANTF-Au is expected due to the occupancy of SAMs on edges and corners of nanostructures. Improved surface coverage of MUA on gold nanoparticles has also been reported previously using inductively coupled plasma–mass spectrometry [35].

3.8. Biosensing

3.8.1. Interactions of OVA and Con A

To prove the ability of PANTF-Au as an effective transducer for biosensing, we chose to study model interaction between glycoprotein OVA and lectin Con A because of their ease of availability, stability, and specificity toward each other. Fig. 8A shows the representative LSPR spectra of PANTF-Au at different modification steps inside flow cell after N_2 dry. The peak wavelength of PANTF-Au modified with SAM of MUA is 539 nm, which shifted to 544 nm on covalently immobilizing OVA through EDC/NHS chemistry. The specific interaction of OVA with Con A shifted the peak wavelength to 550 nm, demonstrating the excellent ability of PANTF-Au for biosensing. We regenerated the functionalized PANTF-Au using previously reported wet-chemical method of cleaning Au, which involves cleaning gold with ethanol, nitric acid and piranha solution in series [1,9]. We did not observe any visible peeling or cracking on the surface and cyclic voltammetry as well as SEM (Figure S4) were used to confirm the regeneration of the surface. Fig. 8B shows the biosensing capacity of the regenerated PANTF-Au used for generating data in Fig. 8A. The LSPR peak wavelength of the regenerated

PANTF-Au at each step of modification is exactly the same as that for freshly prepared PANTF-Au. However, the slight change in reciprocal reflectivity after regeneration is as expected. A similar change in reciprocal reflectivity can also be frequently observed for fresh PANTF-Au when replaced without cleaning. This is another reason why LSPR spectroscopy based on change in reciprocal reflectivity is not the best choice for biosensing applications. It is worth noting that the regeneration of PANTF-Au is also possible using electrochemical techniques, such as by applying different cycles of CV, as shown in Fig. 7B.

3.8.2. *Interactions of SNA and AGP*

Rapid detection of low abundance of biomolecules in a micrometer-sized droplet is of great interest for early diagnosis of disease. Moreover, this type of detection method has huge implications in detecting virus and bacteria in a pandemic or epidemic situation, where quickly detecting an infected person is of utmost importance. We designed a simple setup around the PANTF-Au to create a microwell plate that can be used for a quick drop test of an analyte. Fig. 9A is a photographic image and schematic diagram of the setup, where a 10 μL droplet of a sample can be pipetted inside each microwell plate to detect the analyte. AGP (also known as orosomucoid) is a 41–43 kDa glycoprotein with 45% of the molecular weight represented by glycan in the form of five to six highly sialylated complex-type-*N*-linked glycans [36]. It is an acute phase protein and its concentration in serum elevates in response to infection and inflammation. It is also identified as one of the useful circulating biomarkers for estimating the five-year risk of all-cause mortality [37]. However, its change in concentration in serum does not always provide the specificity of the root cause of the inflammation. Instead, it is believed that change in the nature and types of glycan is linked to disease condition [36]. Using a variety of lectins and studying their interactions with AGP could provide important insights to overcome this problem. As a proof-of-concept, we studied binding affinity of lectin SNA with AGP using drop test method in PANTF-Au. Fig. 9B shows LSPR peak before (530 nm) and after the binding of AGP with SNA (544 nm) that were functionalized on PANTF-Au surface. Fig. 9C is the peak wavelength shift as a function of concentration of AGP and the solid line is fitted with Eq. (1). Using this method, we were able to detect AGP concentration down to few ng/mL with the K_d value of 31.04 μM.

4. Conclusions

We have demonstrated a novel approach to form highly stable thin film of gold on silica wafer without the use of intermediate layer. As-prepared film was utilized to design highly robust PANTF-Au by electrodeposition technique. The PANTF-Au has LSPR spectra in the visible region with a high refractive index sensitivity of 150 nm/RIU and can also be easily integrated with electrochemical techniques. We showed that the PANTF-Au can be used along with a reflection-based LSPR geometry to simplify the biosensing method by studying glycoprotein-lectin interactions. In the scenario of many proof-of-concepts lacking the real-world applications, our results provide the direct, simple and reproducible means for improving biological assay. Detection of native biomolecules in real biological samples using PANTF-Au would be the focus of our future research.

Author contributions

The manuscript was written through contributions of all authors. All authors have given approval to the final version of the manuscript

Declaration of Competing Interest

The authors declare no competing financial interest.

Acknowledgements

The authors gratefully acknowledge financial supports from NIGMS awards R01-GM090254 and R01-GM111835.

Appendix A. Supplementary data

Supplementary material related to this article can be found, in the online version, at doi:https://doi.org/10.1016/j.sna.2020.112155.

References

[1] J.K. Bhattarai, A. Sharma, K. Fujikawa, A.V. Demchenko, K.J. Stine, Electrochemical synthesis of nanostructured gold film for the study of carbohydrate–lectin interactions using localized surface plasmon resonance spectroscopy, Carbohydr. Res. 405 (2015) 55–65.
[2] F. Muench, A. Solomonov, T. Bendikov, L. Molina-Luna, I. Rubinstein, A. Vaskevich, Empowering electroless plating to produce silver nanoparticle films for DNA biosensing using localized surface plasmon resonance spectroscopy, ACS Appl. Bio Mater. 2 (2019) 856–864.
[3] M.D. Susman, Y. Feldman, A. Vaskevich, I. Rubinstein, Chemical deposition and stabilization of plasmonic copper nanoparticle films on transparent substrates, Chem. Mater. 24 (2012) 2501–2508.
[4] K.K. Gopalan, B. Paulillo, D.M. Mackenzie, D. Rodrigo, N. Bareza, P.R. Whelan, et al., Scalable and tunable periodic graphene nanohole arrays for mid-infrared plasmonics, Nano Lett. 18 (2018) 5913–5918.
[5] M.W. Knight, N.S. King, L. Liu, H.O. Everitt, P. Nordlander, N.J. Halas, Aluminum for plasmonics, ACS Nano 8 (2013) 834–840.
[6] H. Reddy, U. Guler, Z. Kudyshev, A.V. Kildishev, V.M. Shalaev, A. Boltasseva, Temperature-dependent optical properties of plasmonic titanium nitride thin films, ACS Photonics 4 (2017) 1413–1420.
[7] J.K. Bhattarai, M.H.U. Maruf, K.J. Stine, Plasmonic-active nanostructured thin films, Processes 8 (2020) 115.
[8] T.H. Chow, N. Li, X. Bai, X. Zhuo, L. Shao, J. Wang, Gold nanobipyramids: an emerging and versatile type of plasmonic nanoparticles, Acc. Chem. Res. 52 (2019) 2136–2146.
[9] J.K. Bhattarai, Y.H. Tan, B. Pandey, K. Fujikawa, A.V. Demchenko, K.J. Stine, Electrochemical impedance spectroscopy study of Concanavalin A binding to self-assembled monolayers of mannosides on gold wire electrodes, J. Electroanal. Chem. 780 (2016) 311–320.
[10] A. Sharma, J.K. Bhattarai, S.S. Nigudkar, S.G. Pistorio, A.V. Demchenko, K.J. Stine, Electrochemical impedance spectroscopy study of carbohydrate-terminated alkanethiol monolayers on nanoporous gold: implications for pore wetting, J. Electroanal. Chem. 782 (2016) 174–181.
[11] M. Schwind, B. Kasemo, I. Zorić, Localized and propagating plasmons in metal films with nanoholes, Nano Lett. 13 (2013) 1743–1750.
[12] M. Couture, L.S. Live, A. Dhawan, J.-F. Masson, EOT or Kretschmann configuration? Comparative study of the plasmonic modes in gold nanohole arrays, Analyst 137 (2012) 4162–4170.
[13] P.L. Stiles, J.A. Dieringer, N.C. Shah, R.P. Van Duyne, Surface-enhanced raman spectroscopy, Annu. Rev. Anal. Chem. 1 (2008) 601–626.
[14] J. Lee, Q. Zhang, S. Park, A. Choe, Z. Fan, H. Ko, Particle–film plasmons on periodic silver film over nanosphere (AgFON): a hybrid plasmonic nanoarchitecture for surface-enhanced Raman spectroscopy, ACS Appl. Mater. Interfaces 8 (2016) 634–642.
[15] P.M. Mendes, S. Jacke, K. Critchley, J. Plaza, Y. Chen, K. Nikitin, et al., Gold nanoparticle patterning of silicon wafers using chemical e-beam lithography, Langmuir 20 (2004) 3766–3768.
[16] M. Veiseh, Y. Zhang, K. Hinkley, M. Zhang, Two-dimensional protein micropatterning for sensor applications through chemical selectivity technique, Biomed. Microdevices 3 (2001) 45–51.
[17] S.J. Madsen, M. Esfandyarpour, M.L. Brongersma, R. Sinclair, Observing plasmon damping due to adhesion layers in gold nanostructures using electron energy loss spectroscopy, ACS Photonics 4 (2017) 268–274.
[18] M.B. Ali, F. Bessueille, J.M. Chovelon, A. Abdelghani, N. Jaffrezic-Renault, M.A. Maaref, et al., Use of ultra-thin organic silane films for the improvement of gold adhesion to the silicon dioxide wafers for (bio)sensor applications, Mater. Sci. Eng. C 28 (2008) 628–632.
[19] L. Leandro, R. Malureanu, N. Rozlosnik, A. Lavrinenko, Ultrathin, ultrasmooth gold layer on dielectrics without the use of additional metallic adhesion layers, ACS Appl. Mater. Interfaces 7 (2015) 5797–5802.
[20] T.G. Habteyes, S. Dhuey, E. Wood, D. Gargas, S. Cabrini, P.J. Schuck, et al., Metallic adhesion layer induced plasmon damping and molecular linker as a nondamping alternative, ACS Nano 6 (2012) 5702–5709.

[21] M. Veiseh, M.H. Zareie, M. Zhang, Highly selective protein patterning on gold-silicon substrates for biosensor applications, Langmuir 18 (2002) 6671–6678.
[22] S.W. Ryu, C.H. Kim, J.W. Han, C.J. Kim, C. Jung, H.G. Park, et al., Gold nanoparticle embedded silicon nanowire biosensor for applications of label-free DNA detection, Biosens. Bioelectron. 25 (2010) 2182–2185.
[23] C. Pacholski, S. Rosencrantz, R.R. Rosencrantz, R.F. Balderas-Valadez, Plasmonic biosensors fabricated by galvanic displacement reactions for monitoring biomolecular interactions in real time, Anal. Bioanal. Chem. (2020).
[24] D. Qin, Y. Xia, G.M. Whitesides, Soft lithography for micro- and nanoscale patterning, Nat. Protocols 5 (2010) 491–502.
[25] D. Li, Z. Shang, Y. She, Z. Wen, Investigation of Au/Si eutectic wafer bonding for MEMS accelerometers, Micromachines 8 (2017) 158.
[26] N. Ferralis, R. Maboudian, C. Carraro, Temperature-induced self-pinning and nanolayering of AuSi eutectic droplets, J. Am. Chem. Soc. 130 (2008) 2681–2685.
[27] H. Sun, M. Yu, G. Wang, X. Sun, J. Lian, Temperature-dependent morphology evolution and surface plasmon absorption of ultrathin gold island films, J. Phys. Chem. C 116 (2012) 9000–9008.
[28] K.M. Mayer, J.H. Hafner, Localized surface plasmon resonance sensors, Chem. Rev. 111 (2011) 3828–3857.
[29] A.J. Haes, R.P. Van Duyne, A nanoscale optical biosensor: sensitivity and selectivity of an approach based on the localized surface plasmon resonance spectroscopy of triangular silver nanoparticles, J. Am. Chem. Soc. 124 (2002) 10596–10604.
[30] J.C. Riboh, A.J. Haes, A.D. McFarland, C.R. Yonzon, R.P. Van Duyne, A nanoscale optical biosensor: real-time immunoassay in physiological buffer enabled by improved nanoparticle adhesion, J. Phys. Chem. B 107 (2003) 1772–1780.
[31] A.V. Whitney, J.W. Elam, S. Zou, A.V. Zinovev, P.C. Stair, G.C. Schatz, et al., Localized surface plasmon resonance nanosensor: a high-resolution distance-dependence study using atomic layer deposition, J. Phys. Chem. B 109 (2005) 20522–20528.
[32] J.A. Jackman, A. Rahim Ferhan, N.-J. Cho, Nanoplasmonic sensors for biointerfacial science, Chem. Soc. Rev. 46 (2017) 3615–3660.
[33] D.A. Gish, F. Nsiah, M.T. McDermott, M.J. Brett, Localized surface plasmon resonance biosensor using silver nanostructures fabricated by glancing angle deposition, Anal. Chem. 79 (2007) 4228–4232.
[34] J.C. Love, L.A. Estroff, J.K. Kriebel, R.G. Nuzzo, G.M. Whitesides, Self-assembled monolayers of thiolates on metals as a form of nanotechnology, Chem. Rev. 105 (2005) 1103–1170.
[35] H. Hinterwirth, S. Kappel, T. Waitz, T. Prohaska, W. Lindner, M. Lämmerhofer, Quantifying thiol ligand density of self-assembled monolayers on gold nanoparticles by inductively coupled plasma–mass spectrometry, ACS Nano 7 (2013) 1129–1136.
[36] T. Fournier, N.N. Medjoubi, D. Porquet, Alpha-1-acid glycoprotein, Biochim. Biophys. Acta 1482 (2000) 157–171.
[37] K. Fischer, J. Kettunen, P. Wurtz, T. Haller, A.S. Havulinna, A.J. Kangas, et al., Biomarker profiling by nuclear magnetic resonance spectroscopy for the prediction of all-cause mortality: an observational study of 17,345 persons, PLoS Med. 11 (2014), e1001606.